A Spectral Vanishing Viscosity Method for Stabilizing Low-Dimensional Galerkin Systems

S. Sirisup and G.E. Karniadakis

Division of Applied Mathematics, Brown University, Providence, RI 02912

Abstract

Low-dimensional flow dynamical systems are susceptible to instabilities after long-time integration. In this paper, we investigate the stability of such two-dimensional models constructed from Karhunen-Loeve expansions for flows past a circular cylinder. We first demonstrate that although the short-term dynamics may be predicted accurately with only a handful of modes retained, instabilities arise after a few hundred vortex shedding cycles. We then propose a dissipative model based on a spectral vanishing viscosity (SVV) diffusion convolution operator as an effective way of stabilizing low-dimensional Galerkin systems.

Key words: Dynamical systems, artificial viscosity, stability, Galerkin projections, non-linear Galerkin, low-dimensional
PACS: 37E99, 65P99

1 Introduction

Proper orthogonal decomposition (POD) is a methodology that first identifies the few most energetic modes in a time-dependent system, and second provides a means of obtaining a low-dimensional description of the system's dynamics [1]. A particular effective approach is the *method of snapshots*, first proposed in [2] for flow systems, that makes the method easy to implement in practice. POD has been successfully implemented in conjunction with experimental (e.g., [3–6,**?**]) as well as with numerical studies (e.g., [7,2,8–12]) in thermal convection, shear layers, cavity flows and external flows, to mention just a few.

* Corresponding Author: G.E. Karniadakis, gk@cfm.brown.edu

Report Documentation Page

Form Approved
OMB No. 0704-0188

1. REPORT DATE	2. REPORT TYPE	3. DATES COVERED
SEP 2002		**00-09-2002 to 00-09-2002**

4. TITLE AND SUBTITLE	5a. CONTRACT NUMBER
A Spectral Vanishing Viscosity Method for Stabilizing Low-Dimensional Galerkin Systems	5b. GRANT NUMBER
	5c. PROGRAM ELEMENT NUMBER
6. AUTHOR(S)	5d. PROJECT NUMBER
	5e. TASK NUMBER
	5f. WORK UNIT NUMBER
7. PERFORMING ORGANIZATION NAME(S) AND ADDRESS(ES) **Brown University,Division of Applied Mathematics,182 George Street,Providence,RI,02912**	8. PERFORMING ORGANIZATION REPORT NUMBER
9. SPONSORING/MONITORING AGENCY NAME(S) AND ADDRESS(ES)	10. SPONSOR/MONITOR'S ACRONYM(S)
	11. SPONSOR/MONITOR'S REPORT NUMBER(S)

12. DISTRIBUTION/AVAILABILITY STATEMENT
Approved for public release; distribution unlimited

13. SUPPLEMENTARY NOTES
The original document contains color images.

14. ABSTRACT

15. SUBJECT TERMS

16. SECURITY CLASSIFICATION OF:			17. LIMITATION OF ABSTRACT	18. NUMBER OF PAGES	19a. NAME OF RESPONSIBLE PERSON
a. REPORT	b. ABSTRACT	c. THIS PAGE			
unclassified	**unclassified**	**unclassified**		**24**	

In some of the aforementioned studies *ad hoc* viscosity models have been incorporated to produce stable simulations (e.g., [11] for cavity flows) while in others there was no explicit stabilization technique incorporated (e.g., [7] for cylinder flows). In particular, as the number of modes increases above a certain threshold the POD-based model seems to be stable at least for short-time integration. The stability of the model, however, is strongly dependent on the flow geometry and regime, while most of the fixes for one flow are not effective in another flow. Also, most of the studies so far have addressed short-term dynamics while instabilities may arise after thousands of convective time units.

From the theoretical standpoint, it is well known that the system of ordinary differential equations derived from the Galerkin projection of a dissipative PDE may be unstable for the long-term dynamics, see [13]. A potential approach to restore dissipation back to the low-dimensional system is *nonlinear Galerkin* projection, which is based on concepts of approximate inertial manifolds, see ([14], [15] and [16]). For fully discrete systems, the nonlinear Galerkin method has been shown to be stable for the long-term dynamics but some sensitivity to initial data was also revealed, see [17]. In practice, this method works effectively as we have recently shown in [18] using a low-dimensional system constructed from experimental (Particle Image Velocimetry) data. However, we have encountered several other reduced flow model systems for which such stabilization proved inadequate. We will demonstrate this behavior in the following.

In this paper, we present an alternative stabilization strategy based on the spectral vanishing viscosity (SVV) method. SVV was first introduced in [19] in the context of constructing *monotonicity preserving* discretizations to hyperbolic conservation laws. More recently, it has been employed successfully in formulating alternative large-eddy simulation (LES) approaches [20]. Also, in [21], the Legendre spectral vanishing method was shown to effectively control the Gibbs phenomenon, while in [22], the SVV approach was employed in two-dimensional simulation of waves in stratified atmosphere.

The spectral vanishing viscosity approach guarantees an essentially non-oscillatory behavior although some small oscillations of *bounded amplitude* may be present in the solution. This theory is based on three key components:

(1) A vanishing viscosity amplitude which decreases with the mode number;
(2) A viscosity-free spectrum for the lower, most energetic modes; and
(3) An appropriate viscosity kernel for the high-wave numbers.

SVV is especially suitable for *hierarchical discretizations* such as the proper orthogonal decomposition where global energetically-ordered modes are involved. This implies that SVV preserves the inherent energetic scale separation while it also maintains monotonicity of the total variation bounded

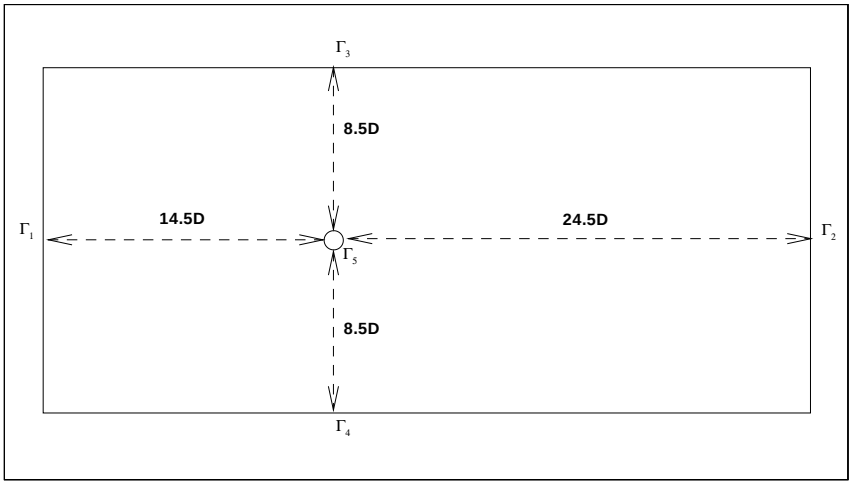

Fig. 1. Computational domain.

(TVB) kind by controlling the high-frequency components. This effective regularization is determined by parameters whose range is given directly by the theory for advection-dominated systems. More recent work has extended the method to superviscosity formulations, first by Tadmor [23] and later by Ma [24,25], in order to extend the range of the *viscosity-free* spectrum.

In the following, we first demonstrate a few cases where instabilities arise and subsequently we introduce the SVV method and present asymptotically stable results by incorporating SVV.

2 Mathematical Formulation

2.1 Direct Numerical Simulation

We consider here flow past a circular cylinder for which both two- and three-dimensional POD models have been constructed in [7] and [26], respectively. These models were stable for tens and even hundreds of shedding cycles without incorporating any stabilization scheme. We will examine the stability of these flows; in particular for the concepts developed here we consider *two-dimensional* uniform flow past a circular cylinder at Reynolds number $Re = 100$ and $Re = 500$.

The computational domain is shown in figure 1. Uniform steady or time-dependent boundary conditions are imposed at the inflow boundary Γ_1. Uniform velocity is also imposed on Γ_3 and Γ_4 while on Γ_2 the zero Neumann condition on velocity is imposed. On the cylinder surface Γ_5 the no-slip boundary condition is prescribed. Converged solutions were obtained using the spectral/hp

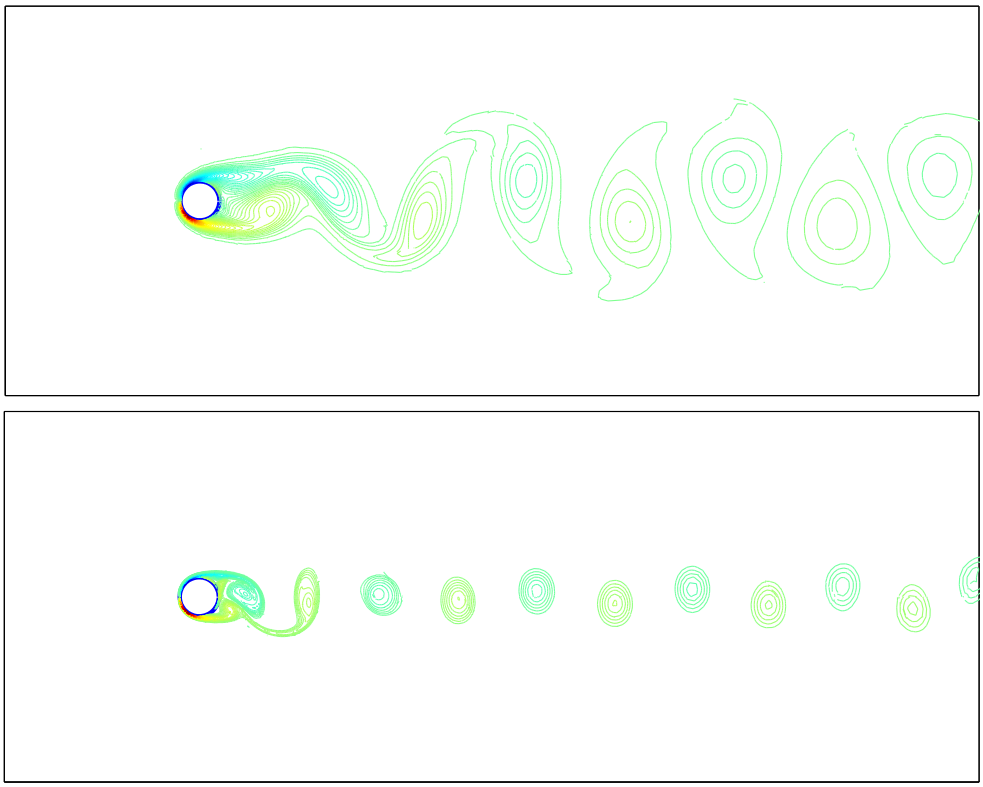

Fig. 2. Instantaneous vorticity contours at Re=100 (upper) and Re=500 (lower).

element method [27]. Typical results that show the differences in spatial scales in terms of vorticity at Re=100 and $Re = 500$ are shown in figure 2.

2.2 POD Models

We employed 50 snapshots of DNS data in order to construct the low-dimensional models using the proper orthogonal decomposition. We briefly review this procedure next.

Let us decompose the total flow field $\mathbf{V}$ as

$$\mathbf{V}(\mathbf{x}, t) = \mathbf{U_0}(\mathbf{x}) + \mathbf{u}(\mathbf{x}, t)$$

where $\mathbf{U_0}$ is the *time-averaged* field.

Then, we extract the POD modes, based on the DNS data, which are eigenvectors of a covariance matrix $\mathbf{C}$; its elements are computed as follows

$$c_{i,j} = \imath\mathbf{u}(\mathbf{x},t_i)\cdot\mathbf{u}(\mathbf{x},t_j)d\mathbf{x} = \int\Big(u(x,y,t_i)u(x,y,t_j)+v(x,y,t_i)v(x,y,t_j)\Big)dx\,dy\,,$$

where u, v are the two components of the velocity vector $\mathbf{u}$. This is the *snap-*

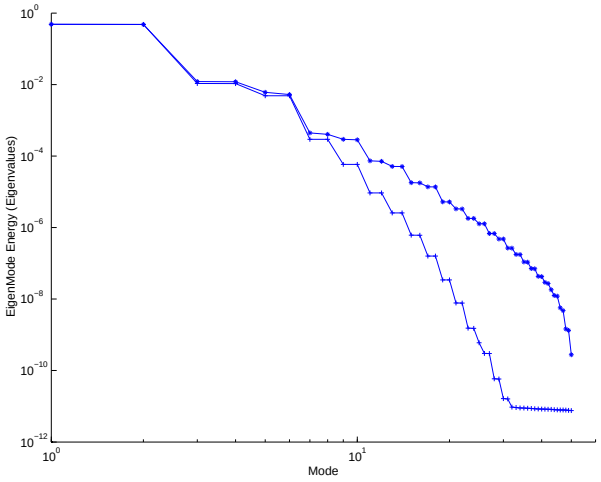

Fig. 3. POD eigenvalues for $Re = 100$ $(+)$ and $Re = 500$ $(*)$.

shot method formulation, see [28–30]. The matrix $\mathbf{C}$ represents the correlation between temporal points since the spatial variable has been integrated out. We then compute the eigenvectors of the above covariance matrix, denoted by $\mathbf{a}$, and the POD modes denoted by $\boldsymbol{\phi}(x, y)$. Specifically, the vector $\boldsymbol{\phi}(x, y)$ is given by

$$\phi_u(x, y)_j = \sum_{i=1}^{N} a_j(t_i) u(x, y, t_i)$$

$$\phi_v(x, y)_j = \sum_{i=1}^{N} a_j(t_i) v(x, y, t_i)$$

where N is the total number of snapshots, ϕ_u and ϕ_v are the components of the vector $\boldsymbol{\phi}(x, y)$, and j is the mode index. The corresponding eigenvalues are ordered and plotted in figure 3 for $Re = 100$ and $Re = 500$.

We employ the hierarchical POD modes obtained from the DNS data as a basis to represent the velocity field. In addition, we employ a Galerkin projection of the Navier-Stokes equations onto spatial modes to obtain the system of ordinary differential equation that governs the dynamics of the system.

We express the two-dimensional field $\mathbf{u}$ as the linear combination of the POD modes

$$u(x, y, t) = \sum_{j=1}^{N} \phi_u(x, y)_j a_j(t),$$

$$v(x, y, t) = \sum_{j=1}^{N} \phi_v(x, y)_j a_j(t),$$

where $a_j(t)$ are the unknown coefficients. The Galerkin projection of the Navier-Stokes equations gives

$$\int \boldsymbol{\phi} \cdot \left(\frac{\partial \mathbf{V}}{\partial t} + (\mathbf{V} \cdot \nabla)\mathbf{V} + \nabla p - \frac{1}{R_e}\nabla^2 \mathbf{V} \right) d\mathbf{x} = 0 \tag{1}$$

where the projection vector is $\boldsymbol{\phi} = [\phi_u, \phi_v]^T$, extracted from DNS. We use the divergence-free eigenmodes so the pressure term inside the domain is eliminated via integration by parts. Also the Dirichlet and the outflow conditions imposed at the boundaries lead to the vanishing of contributions from the pressure on those boundaries in the integration by parts procedure.

The Galerkin projection leads to the dynamical system:

$$\frac{\partial a_j(t)}{\partial t} = f(\mathbf{a}) \tag{2}$$

with $\mathbf{a} = [a_1, a_2, \ldots]$. The term $f(\mathbf{a})$ includes the convective and viscous terms and has the form:

$$\begin{aligned} f(\mathbf{a}) = & -\left(\int \boldsymbol{\phi}_j \nabla \cdot (\boldsymbol{\phi}_i \boldsymbol{\phi}_k) d\mathbf{x} \right) a_i a_k \\ & - \left(\frac{1}{Re} \int \nabla \boldsymbol{\phi}_j \nabla \boldsymbol{\phi}_i d\mathbf{x} + \int \boldsymbol{\phi}_j \nabla \cdot (\boldsymbol{\phi}_i \mathbf{U_0}) d\mathbf{x} + \int \boldsymbol{\phi}_j \nabla \cdot (\mathbf{U_0} \boldsymbol{\phi}_i) d\mathbf{x} \right) a_i \\ & - \left(\int \boldsymbol{\phi}_j \nabla \cdot (\mathbf{U_0} \mathbf{U_0}) d\mathbf{x} + \frac{1}{Re} \int \nabla \boldsymbol{\phi}_j \nabla \mathbf{U_0} d\mathbf{x} \right). \end{aligned}$$

In the following we investigate the time evolution of the modal coefficients $a_j(t)$, $j = 1, 2, \ldots$; we also refer to a_j as the "mode" j.

3 Instability of POD Flow Models

First we present results from the long-time integration of the $Re = 100$ case with steady uniform inflow. It was found in [7] that a 6-mode POD system gives accurate results in comparisons with the original DNS data, at least for the short-time dynamics. Indeed, various reduced models we tested again with $N \geq 6$ are stable after short-time integration, and in fact for times up to several hundreds of shedding cycles. Our experiments, however, show that all models are asymptotically unstable. For example, a 6-mode model is steady for to to 40 shedding cycles (about 200 convective time units) as shown in figure 4 but it diverges for time $t > 200$. As the number of modes increases the stability of the model is enhanced. So, a 10-mode model is stable for up to

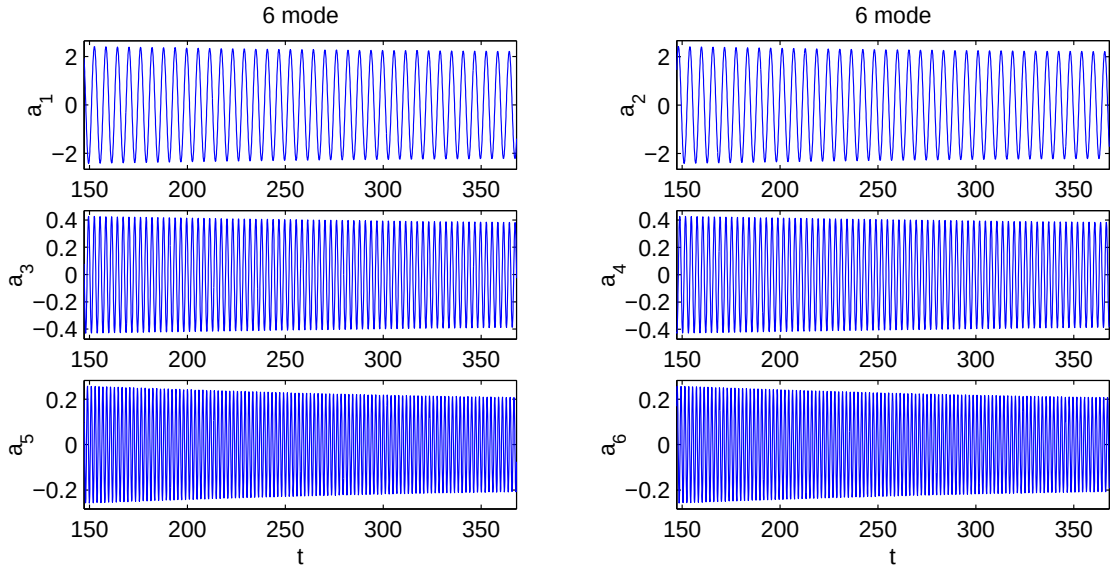

Fig. 4. Re=100: Time history showing the onset of instability (bifurcation) in the 6-mode POD model.

500 shedding cycles, i.e. more than 3,000 convective time units, but eventually all modes diverge as shown in figure 5. In particular, a bifurcation to a new asymptotic state is shown. However, for the first 50 shedding cycles the POD predictions are in very good agreement with the DNS data as shown in figure 6.

The exact onset of instability depends on the number N of modes retained in the reduced model as well as on the Reynolds number. At the higher Reynolds number ($Re = 500$) the onset of instability arises earlier even for a higher-order model. For example, in figure 7 we show the time history of the modes for a 20-mode POD model. The instability here sets in at about 100 shedding cycles into the time integration. This result is typical of several other models we constructed for the uniform steady inflow.

However, not all low-dimensional systems are asymptotically unstable. Our experiments show that *forced systems*, i.e. systems with an imposed time scale through external forcing, may be stable at *all* times. To this end, we consider the flow past a cylinder again at $Re = 500$ but with a small sinusoidal velocity component added at the inflow, with 10% amplitude forced at the Strouhal frequency. The resulting POD system predicts the expected lockin state, in agreement with DNS, and it is stable [31]. In figure 8 we show the time history for the same set up and parameters as in figure 7. It shows stability at the time of the instability onset of the flow described in 7 but also at much longer times (not shown here). The Galerkin model in the unsteady inflow case is based on a modification of the system of equations (2) to include a penalty term that facilitates the time-dependent boundary conditions in the reduced POD system.

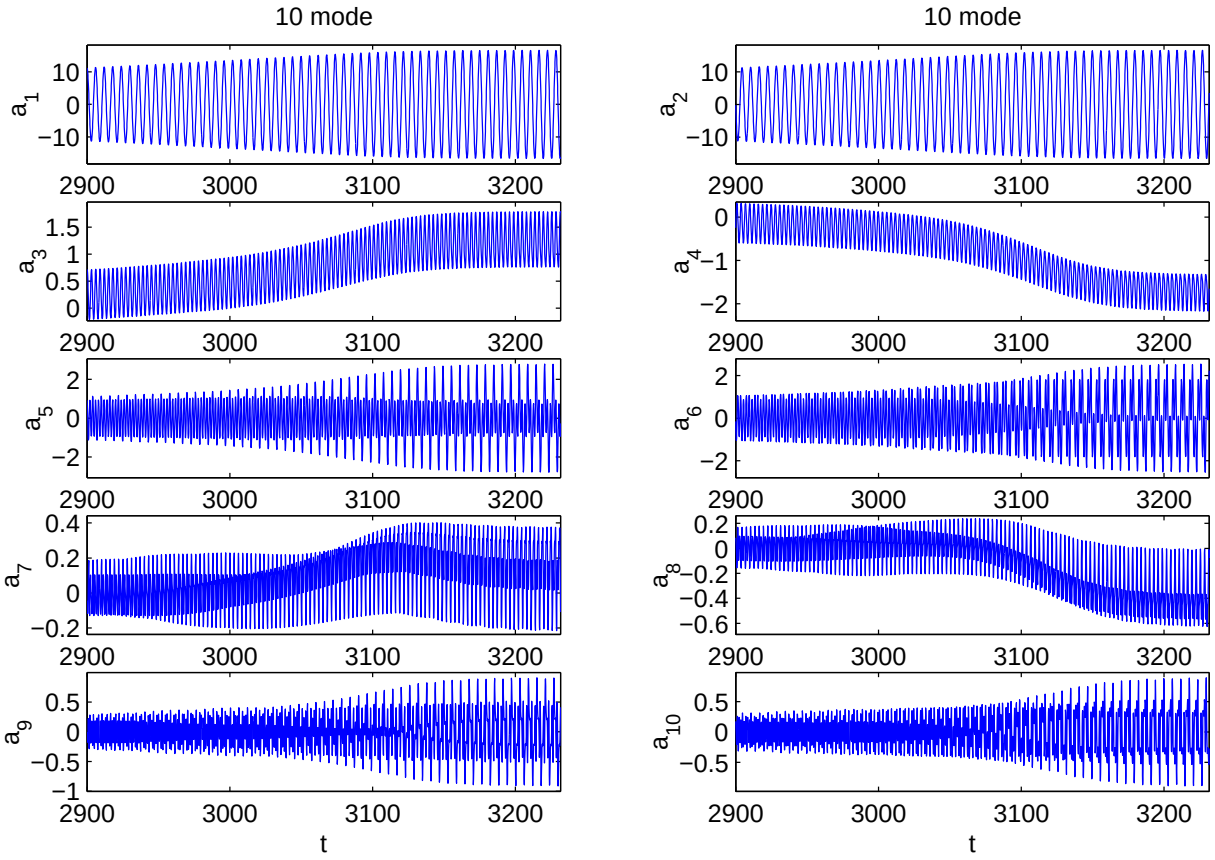

Fig. 5. Re=100: Time history showing the onset of instability (bifurcation) in the 10-mode POD model.

4 The Spectral Vanishing Viscosity Model

Tadmor [19] first introduced the concept of spectral vanishing viscosity (SVV) using the inviscid Burgers' equation

$$\frac{\partial}{\partial t}u(x,t) + \frac{\partial}{\partial x}\left(\frac{u^2(x,t)}{2}\right) = 0, \tag{3}$$

subject to given initial and boundary conditions. The distinct feature of solutions to this problem is that spontaneous jump discontinuities (shock waves) may be developed, and hence *a class* of weak solutions can be admitted. Within this class, there are many possible solutions, and in order to single out the physically relevant one an additional entropy condition is applied, of the form

$$\frac{\partial}{\partial t}\left(\frac{u^2(x,t)}{2}\right) + \frac{\partial}{\partial x}\left(\frac{u^3(x,t)}{3}\right) \leq 0. \tag{4}$$

In low-dimensional systems it has been found that unstable behavior is asociated with multiple spurious steady states [13], and this is consistent with the

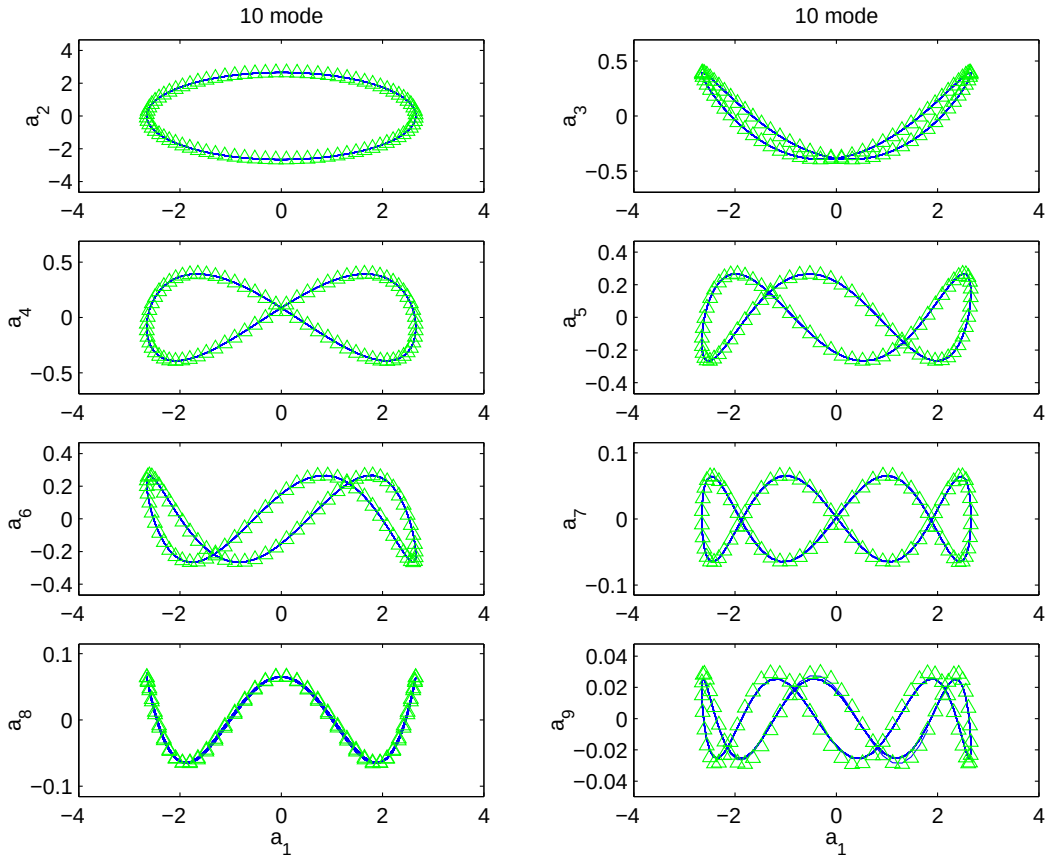

Fig. 6. Re=100: Phase portrait for the first 50 shedding cycles for the 10-mode model. The lines denote POD predictions and the triangles DNS data.

above observation. Tadmor (1989) introduced the spectral vanishing viscosity method, which adds a small amount of *mode-dependent* dissipation that satisfies the entropy condition, yet retains spectral accuracy. It is based on viscosity solutions of nonlinear Hamilton-Jacobi equations, which have been studied systematically in [32]. Specifically, the viscosity solution for the Burgers' equation has the form

$$\frac{\partial}{\partial t}u(x,t) + \frac{\partial}{\partial x}\left(\frac{u^2(x,t)}{2}\right) = \epsilon\frac{\partial}{\partial x}\left[Q_\epsilon \frac{\partial u}{\partial x}\right], \tag{5}$$

where $\epsilon(\to 0)$ is a viscosity amplitude and Q_ϵ is a viscosity kernel. Convergence may then be established by compactness estimates combined with entropy dissipation arguments [19]. To respect spectral accuracy, the SVV method makes use of viscous regularization and equation (5) may be rewritten in discrete form (retaining N modes) as in our POD model

$$\frac{\partial}{\partial t}u_N(x,t) + \frac{\partial}{\partial x}\left[\mathcal{P}_N\left(\frac{u^2(x,t)}{2}\right)\right] = \epsilon\frac{\partial}{\partial x}\left[Q_N * \frac{\partial u_N}{\partial x}\right], \tag{6}$$

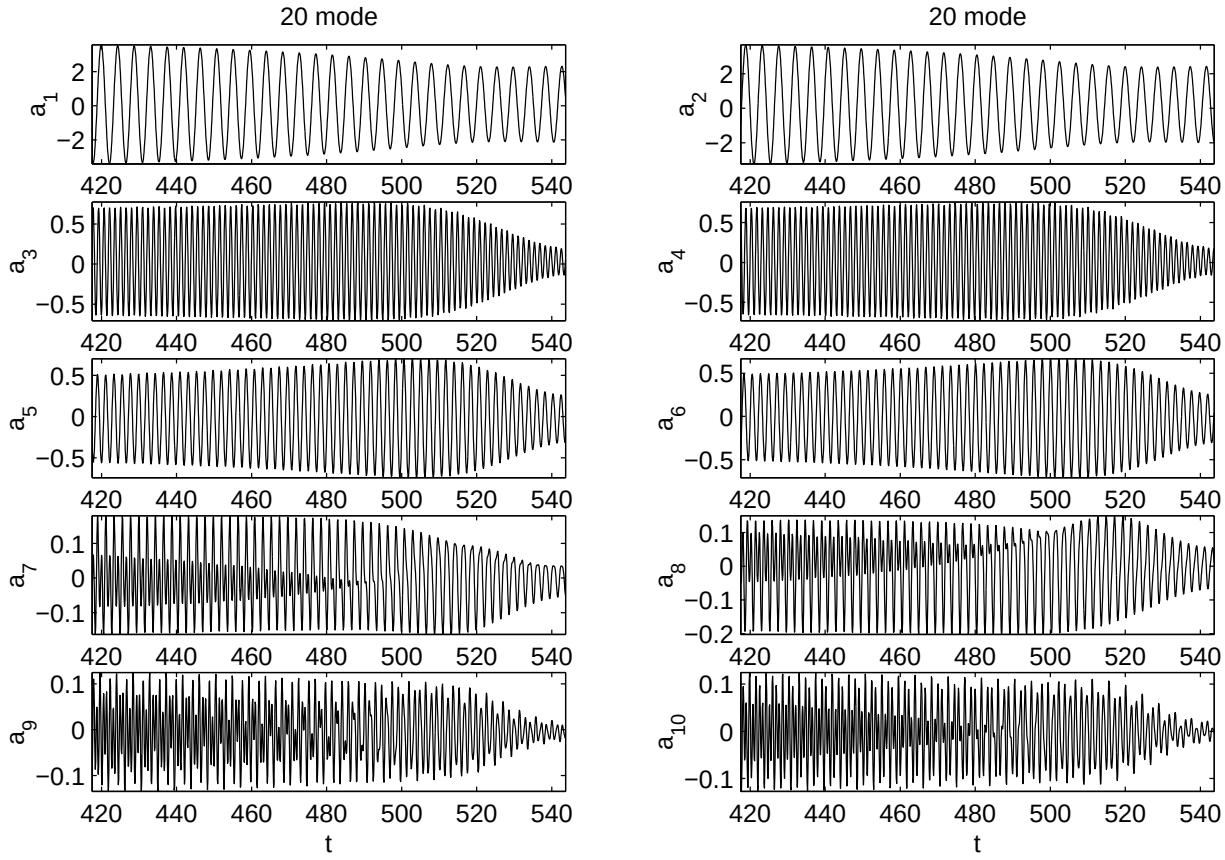

Fig. 7. Re=500; *steady inflow*: Time history showing the onset of instability (bifurcation) in the 20-mode POD model.

where the star ($*$) denotes convolution and $\mathcal{P}_N$ is a projection operator. Q_N is a viscosity kernel, which is only activated for high wave numbers. In Fourier space, this kind of spectral viscosity can be efficiently implemented as multiplication of the Fourier coefficients of u_N with the Fourier coefficients of the kernel Q_N, i.e.,

$$\epsilon \frac{\partial}{\partial x}\left[Q_N * \frac{\partial u_N}{\partial x}\right] = -\epsilon \sum_{M \leq |k| \leq N} k^2 \hat{Q}_k(t)\hat{u}_k(t)e^{ikx},$$

where k is the wave number, N the number of Fourier modes, and M the wavenumber above which the spectral vanishing viscosity is activated. In the POD context, we also assume that this implementation of convolution is valid in the modal space.

Originally, Tadmor (1989) used

$$\hat{Q}_k = \begin{cases} 0, \mid k \mid \leq M \\ 1, \mid k \mid > M, \end{cases} \tag{7}$$

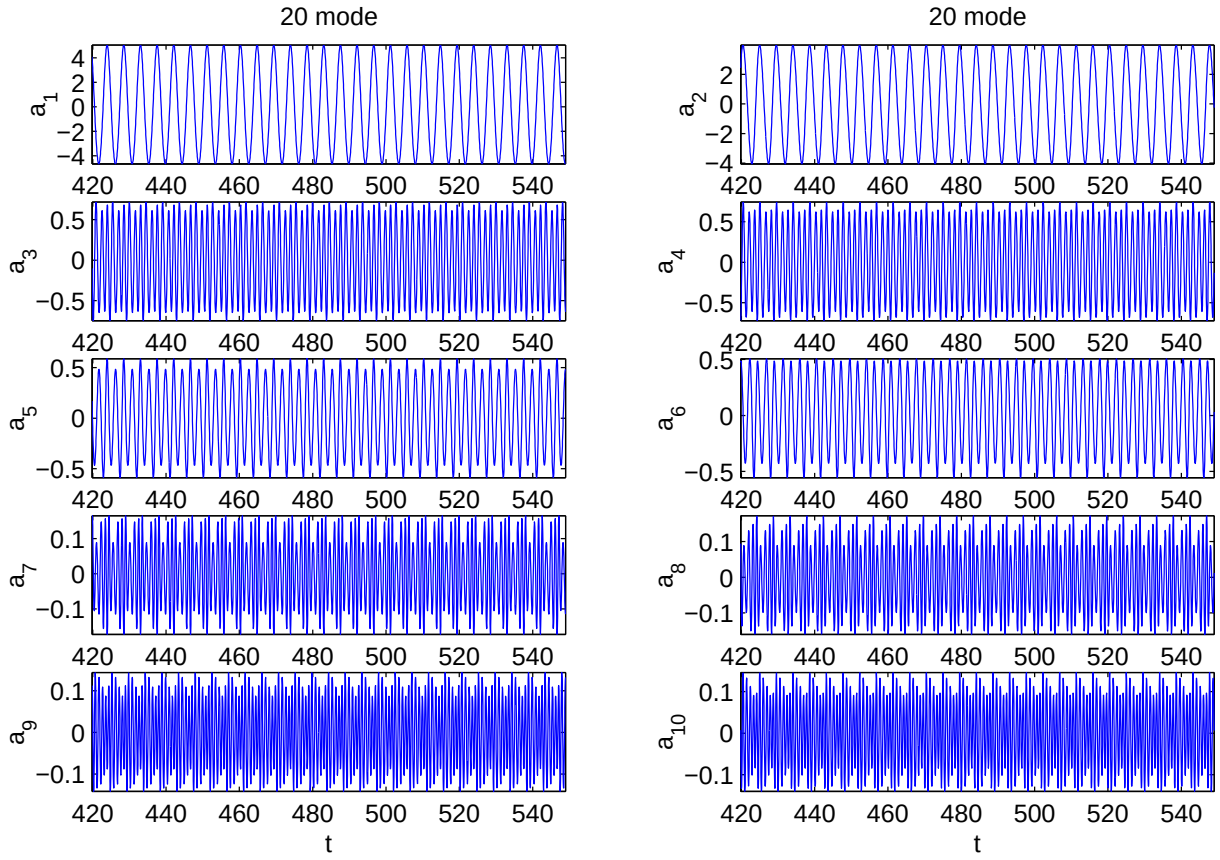

Fig. 8. Re=500; *oscillatory inflow*: Time history showing stability for the 20-mode POD model.

with $\epsilon M \sim 0.25$ based on the consideration of minimizing the total-variation of the numerical solution. In subsequent work, however, a smooth kernel was used, since it was found that the C^∞ smoothness of $\hat{Q}_k$ improves the resolution of the SVV method. For Legendre pseudo-spectral methods, Maday et al. [33] used $\epsilon \approx N^{-1}$, activated for modes $k > M \approx 5\sqrt{N}$, with

$$\hat{Q}_k = e^{-\frac{(k-N)^2}{(k-M)^2}}, \quad k > M. \tag{8}$$

In order to see the difference between the convolution operator on the right-hand-side in equation (6) and the usual viscosity regularization, following Tadmor [34], we expand as

$$\epsilon \frac{\partial}{\partial x}\left[Q_N * \frac{\partial u_N}{\partial x}\right] = \epsilon \frac{\partial^2 u_N}{\partial x^2} - \epsilon \frac{\partial}{\partial x}[R_N(x,t) * \frac{\partial u_N}{\partial x}] \tag{9}$$

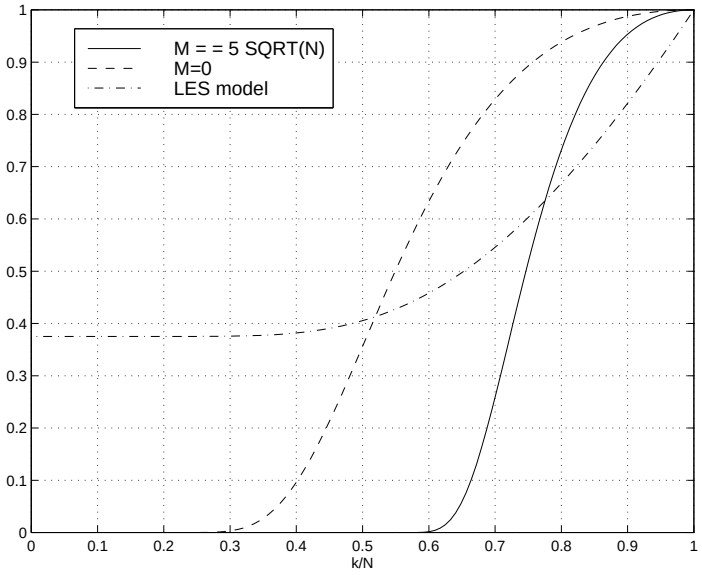

Fig. 9. Normalized viscosity kernels for the spectral vanishing viscosity (dash line $C = 0$ and solid line $C = 5$) and the Kraichnan/Chollet-Lesieur viscosity (dash-dot line).

where

$$R_N(x,t) \equiv \sum_{k=-N}^{N} \hat{R}_k(t) e^{ikx}; \quad \hat{R}_k(t) \equiv \begin{cases} 1 - \hat{Q}_k(t) & |k| \geq M \\ 1 & |k| < M \end{cases} \tag{10}$$

The extra term appearing in addition to the first standard viscosity term makes this method different. It measures the distance between the spectral (vanishing) viscosity and the standard viscosity. This term is bounded in the L_2 norm similarly to the spectral projection error. In this paper we refer to the viscosity as vanishing as the theory requires that

$$\epsilon \approx \frac{1}{N^{\theta} log N}, \quad \theta \leq 1$$

and thus $\epsilon \to 0$ for the high-resolution limit.

At this point it is also instructive to compare the spectral vanishing viscosity to the aforementioned spectral eddy-viscosity introduced by Kraichnan [35] and modified by Chollet-Lesieur [36,37]. The latter has the non-dimensional form [37]

$$\nu(k/N) = K_0^{-3/2}[0.441 + 15.2 exp(-3.03N/k)], \quad K_0 = 2.1 \tag{11}$$

Comparing the Fourier analog of this eddy-viscosity employed in LES [36] to the viscosity kernel $Q_k(k, M, N)$ introduced in the SVV method, figure 9 shows both viscosity kernels normalized by their maximum value at $k = N$.

For SVV two different values of the cut-off wavenumber are considered, i.e.,

$$M = C\sqrt{N} \quad \text{for } C = 0 \text{ and } C = 5, \tag{12}$$

and are shown in the plot of figure 9. In particular, the solid line can be thought of as a *stability barrier* above which monotonicity and thus stability is not guaranteed. On the other hand, the dash line can be thought of as an *accuracy barrier* below which the convergence of the method is affected. This range has been used in most of the numerical experiments so far (see for example [33],[22],[20]) and is consistent with the theoretical results [19]. In the plot it is shown that, in general, the two forms of viscosity have similar distributions but the SVV form does not affect the first one-third or one-half of the spectrum (viscosity-free portion) and it increases faster than the Kraichnan/Chollet-Lesieur eddy-viscosity in the higher wave numbers range, e.g. in the second-half of the spectrum.

The implementation of the SVV in the POD models (equation (2)) is similar to the implementation of Fourier methods presented above or the spectral/*hp* element discretization in [20]. In particular, the system of ordinary differential equations is enhanced as follows

$$\frac{\partial a_j(t)}{\partial t} = f(\mathbf{a}) - h(\mathbf{a}), \tag{13}$$

where $f(\mathbf{a})$ has the form presented in equation (3), and $h(\mathbf{a})$ contains the viscosity convolution kernel, i.e.

$$h(\mathbf{a}) = \epsilon \hat{Q}_j \left[\int \frac{\partial \mathbf{U_0}}{\partial x} \frac{\partial \boldsymbol{\phi}_j}{\partial x} d\mathbf{x} + \sum_{i=1}^{N} a_i(t) \int \frac{\partial \boldsymbol{\phi}_i}{\partial x} \frac{\partial \boldsymbol{\phi}_j}{\partial x} d\mathbf{x} \right]. \tag{14}$$

In this derivation, integration by parts is used and the fact that boundary contributions vanish because of the specific boundary conditions employed. In view of equation (14), we can see that only the higher modes, i.e. mode numbers greater than M, will be affected by the viscosity kernel.

In order to contrast the effect of SVV to simply adding artificial viscosity in the POD model we have also performed simulations with model; the total (non-dimensional) viscosity in this case is mode-dependent and given by

$$\nu_k = \begin{cases} \frac{1}{Re} & k \leq M \\ \frac{1}{Re} + C \exp^{-(\frac{k-N}{k-M})^2} & k > M \end{cases} \tag{15}$$

where, M is the cut-off wavenumber as before and C is a constant.

Re(modes used)	Artificial Viscosity		Spectral Vanishing Viscosity	
	Cut-off (M)	Constant (C)	Cut-off (M)	Constant (ϵ)
100 (6 modes)	4	0.008333	4	0.0137
100 (10 modes)	6	0.04	6	0.00822
500 (6 modes)	2	0.083333	2	0.24167
500 (12 modes)	8	0.166666	10	0.12954961443
500 (20 modes)	n/a	n/a	16	0.0320520703

Table 1
Parameters used in the stabilization schemes.

This artificial viscosity model is chosen to have the exponential effect that SVV has, so to that the higher modes affected the most.

5 Stability of SVV-POD Flow Models

Here we demonstrate the stabilization effect of SVV by revisiting the flow examples already presented in section 2 for cylinder flow. The parameters of the SVV model were chosen guided by the theoretical estimates and also by obtaining the *best agreement* with the original data for the first 50 shedding cycles. A summary of the parameters used is presented in table 1.

We first consider the case $Re = 100$ and examine the phase portraits obtained for all modes for the *first 1000 shedding cycles*. The model with the smallest number of modes that predicts accurately the short-term dynamics corresponds to $N = 6$. However, over the span of 1000 shedding cycles there is loss of stability of this specific model as mentioned earlier (see figure 4). In figure 10 we show the phase portrait corresponding to the first 1000 shedding cycles; clearly the initial good agreement with the DNS data is eventually lost. Stability is recovered, however, if the SVV correction is incorporated. In figure 11 we plot again the phase portrait (over 1000 shedding cycles) of the 6-mode system with the SVV model included. We see that a stable limit cycle is established in agreement with the DNS data.

Similar results are valid for the models with higher modes. Here, we compare the two viscosity formulations to illustrate what is different with SVV. In figure 12 we first show the results for the 10-mode POD system using the *artificial viscosity* for stabilization. In figure 13, we present the same results but with the *SVV model* employed. We see that the agreement of the POD predictions with the DNS original data is *uniformly good* for all modes in contrast with the artificial viscosity model. The latter shows a small divergence which is even greater at longer times (not shown here). Also, the higher modes are

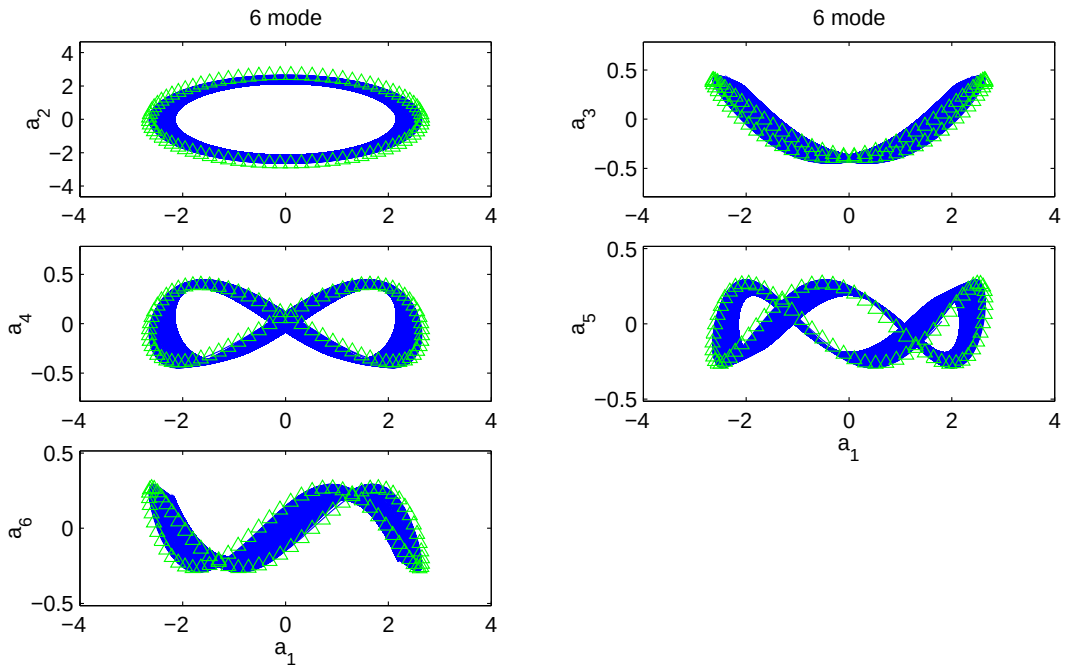

Fig. 10. Re=100: Phase portrait for the 6-mode model without explicit dissipation. The lines denote POD predictions and the triangles DNS data.

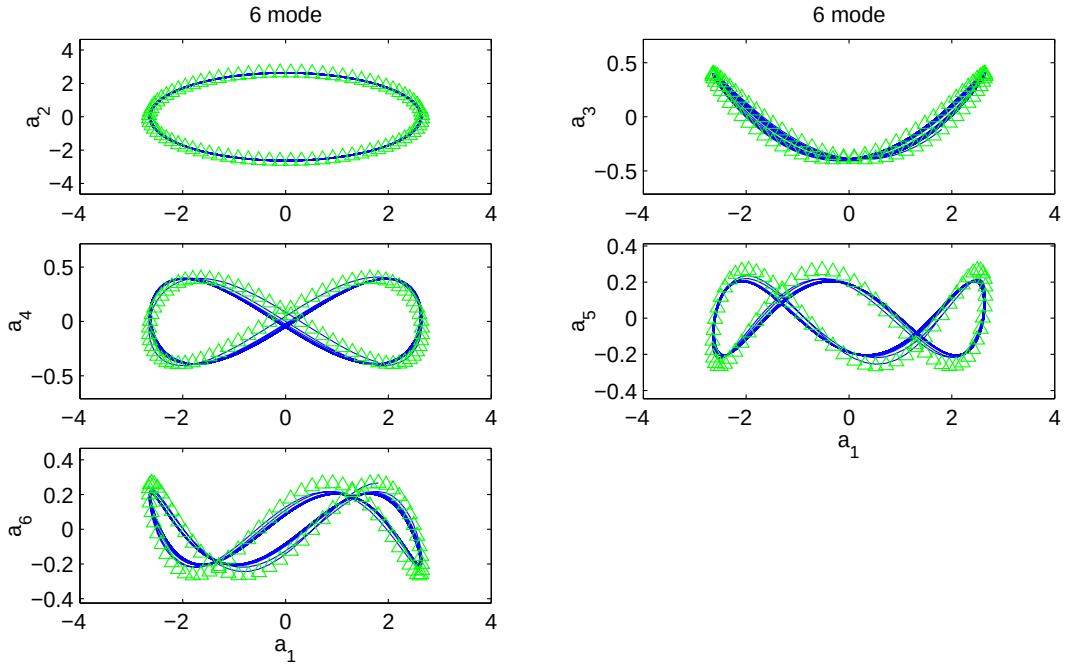

Fig. 11. Re=100: Phase portrait for the 6-mode model with SVV. The lines denote POD predictions and the triangles DNS data.

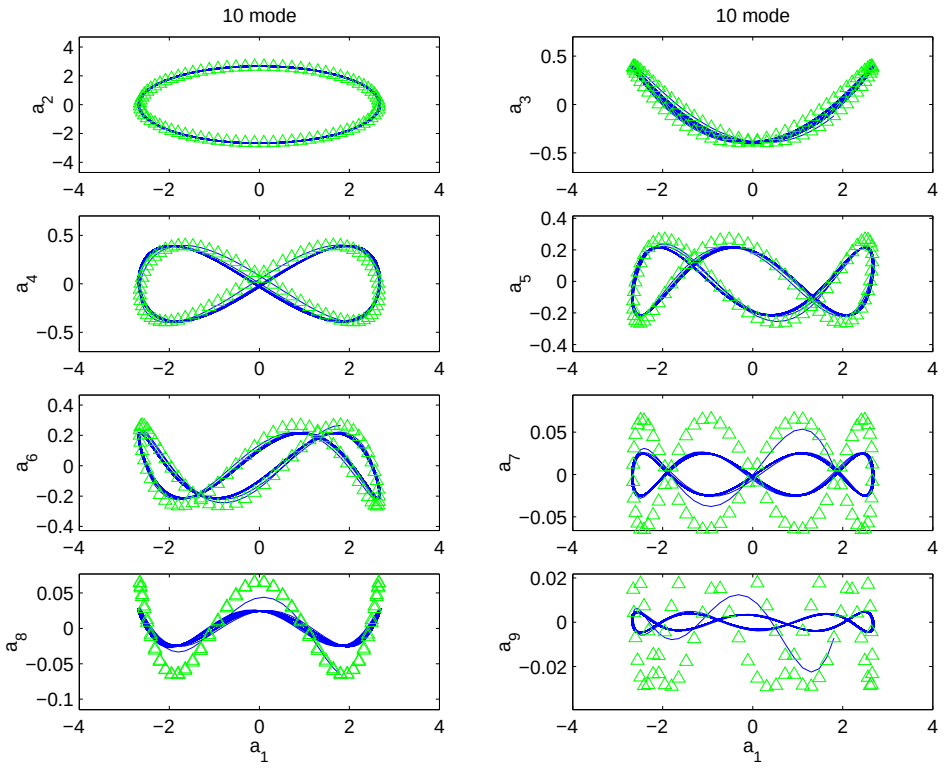

Fig. 12. Re=100: Phase portrait for the 10-mode model using the artificial viscosity model. The lines denote POD predictions and the triangles DNS data.

excessively damped. In order to compare the stabilization of this technique with the stabilization effect of the *nonlinear Galerkin method*, we plot in figure 14 corresponding results from a nonlinear Galerkin model, see [38] for details. The nonlinear Galerkin model is constructed based on *six dominus* (also known as masters) and *four servus* (also known as slaves) POD modes. We see from the phase portrait that this approach is inadequate in obtaining asymptotically stable results although it has improved the results compared to Galerkin-only projection. The same conclusions have been obtained from results with several other dominus-servus combinations not shown here.

For the higher Reynold number, $Re = 500$, for which the POD Galerkin system bifurcates at earlier times SVV can effectively stabilize the simulation. In figure 15 we plot the phase portrait of the first nine modes for the *first 1000 shedding cycles* in the simulation. We see that a limit cycle is predicted in excellent agreement with the DNS data. To appreciate the effect of SVV in the current simulation we also present in figure 16 the corresponding results without SVV from the pure POD Galerkin system for the same time period, which clearly diverges. In this case the cut-off mode was set to $M = 16$ and the viscosity kernel $\epsilon = C/N$ was set as shown in table 5. Using the artificial viscosity approach to stabilize the POD Galerkin model does not lead to accurate results.

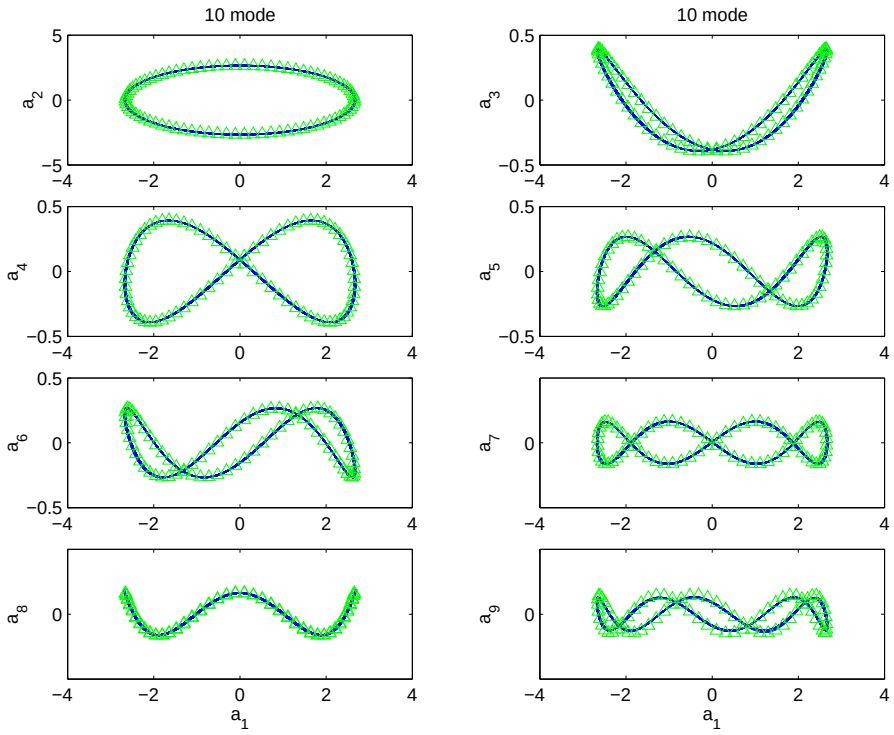

Fig. 13. Re=100: Phase portrait for the 10-mode model using the SVV model. The lines denote POD predictions and the triangles DNS data.

In order to also investigate the effect of SVV on the higher modes we plot separately in figures 17 and 18 the phase portraits up to the 17-th and 20-th mode, respectively. We see that after the cut-off mode $M = 16$ some inaccuracies are introduced, which are more pronounced in the modes 18, 19 and 20. However, the amplitude of those modes is bounded at all times in contrast to the high POD modes of the reduced system without stabilization.

Finally, we note that even lower dimensional systems at $Re = 500$ with truncations corresponding to $N = 6$ and $N = 12$ are stable and give accurate results for the SVV parameters shown in table 5.

6 Summary and Discussion

We have developed a new approach to stabilizing reduced order models derived from Galerkin projections of evolution equations. Specifically, here we have considered the external flow past a cylinder and investigated the stability of the limit (shedding) cycle obtained from a POD-based Galerkin system at two values of Reynolds number. We have found that in the current long-term time integration employed all Galerkin models are asymptotically unstable. However, in previous similar studies, where short to modest length time in-

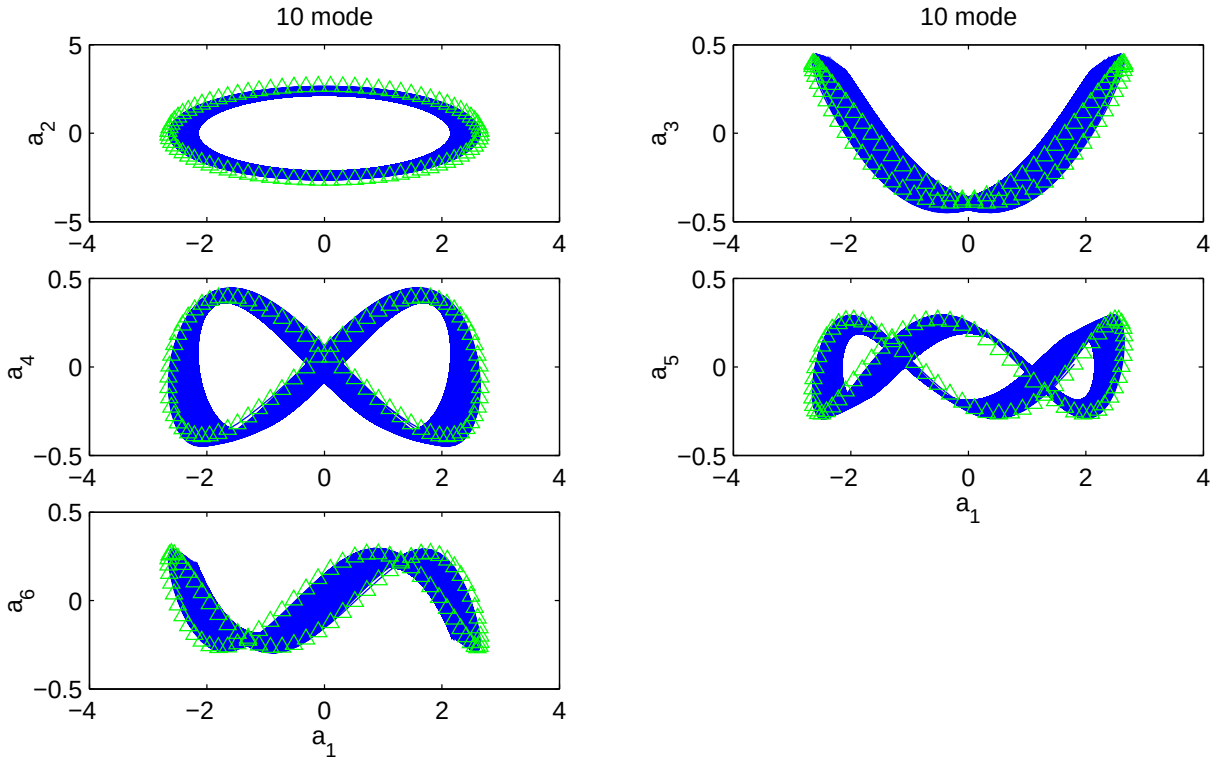

Fig. 14. Re=100: Phase portrait for the 10-mode model using the nonlinear Galerkin method. The lines denote POD predictions and the triangles DNS data.

tegration was involved, it was assumed that such models are asymptotically stable. This instability does not always manifest itself as an explosive growth that leads to blow-up but as a bifurcation that leads to another limit cycle. The precise onset of this bifurcation depends on the number of modes retained in the model and the Reynolds number as well as the flow geometry.

The classical way of incorporating artificial viscosity to stabilize low-order models does not guarantee stability and affects greatly the accuracy of the solution. On the other hand, nonlinear Galerkin projection, although potentially effective for the right combination of *dominus-servus* modes, is not robust; in the cases we considered here it simply prolonged the onset of the instability. The spectral vanishing viscosity (SVV) method we implemented is an effective and robust stabilization scheme. It employs a convolution viscosity kernel, which is parametrized by a viscosity amplitude and a cut-off wavenumber. The theory does not give the precise values of these parameters but provides a stability range in terms of barriers. Above a certain value of the cut-off no stability is guaranteed whereas below a low threshold the accuracy of the low most energetic modes is affected. The viscosity amplitude scales inversely proportional to the mode number, i.e. $\propto C/N$, where the constant C is problem dependent. Here it was chosen on the basis of matching the model's short-term dynamics with the original data.

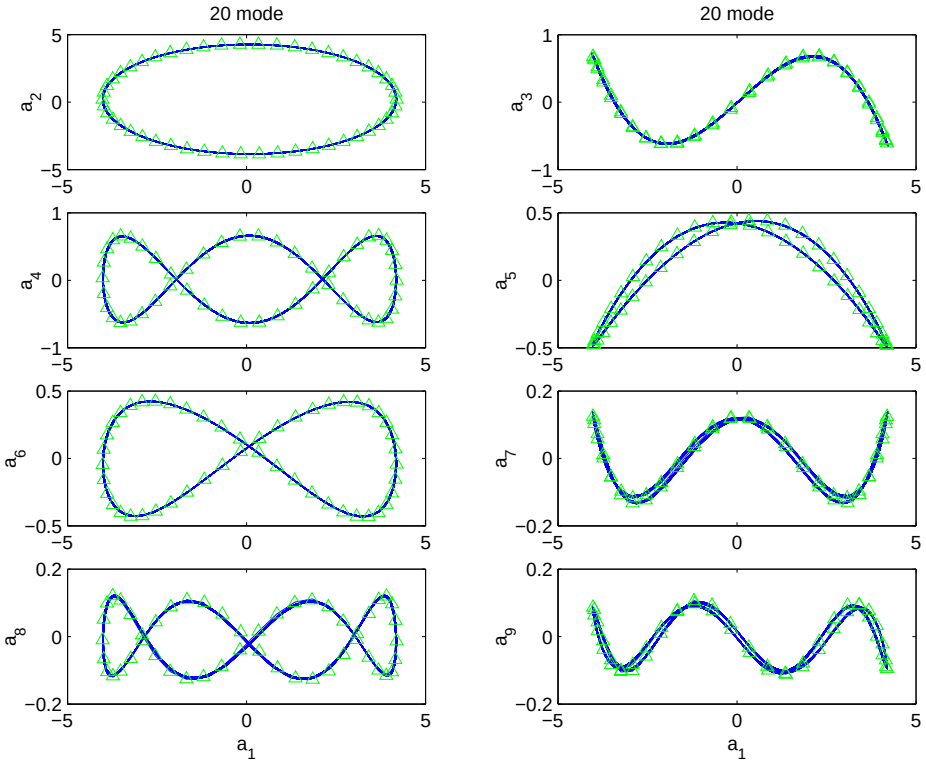

Fig. 15. $Re = 500$: Phase portrait of the first 9 modes in the 20-mode SVV-POD system (lines) compared to the DNS data (symbols).

We have defined here asymptotic stability as stability for the first 1000 shedding cycles somewhat arbitrarily. It is possible that after a much longer time interval an instability is developed. To this end, we investigated this question and found that for the 6-mode system, which can be integrated easily for very long time, stability was achieved for more than 1.25 million convective time units. For the other models some small divergence was detected after several thousands of shedding cycles but a small change in the SVV parameters could improve the results. Clearly, more theoretical work is needed towards this direction to provide simple guidelines to the practitioners of this method.

The SVV nonlinear stability theory is based on the treatment of the inviscid Burgers equation originally proposed by Tadmor [19] for Fourier discretization. We can justify its use in the current context only heuristically and have been motivated by success in other applications [22,20]. However, a rigorous justification for low-dimensional models derived from Galerkin projections is currently missing and thus we do not have much insight into the effectiveness of SVV. The extra term appearing in equation (9), in addition to the standard viscosity term, is perhaps the key but its optimum form may depend on the specific dissipative PDE considered. Future work should address these issues, and also investigate the dissipation spectrum in detail for larger systems with higher number of modes so that a sufficient dissipation range exists.

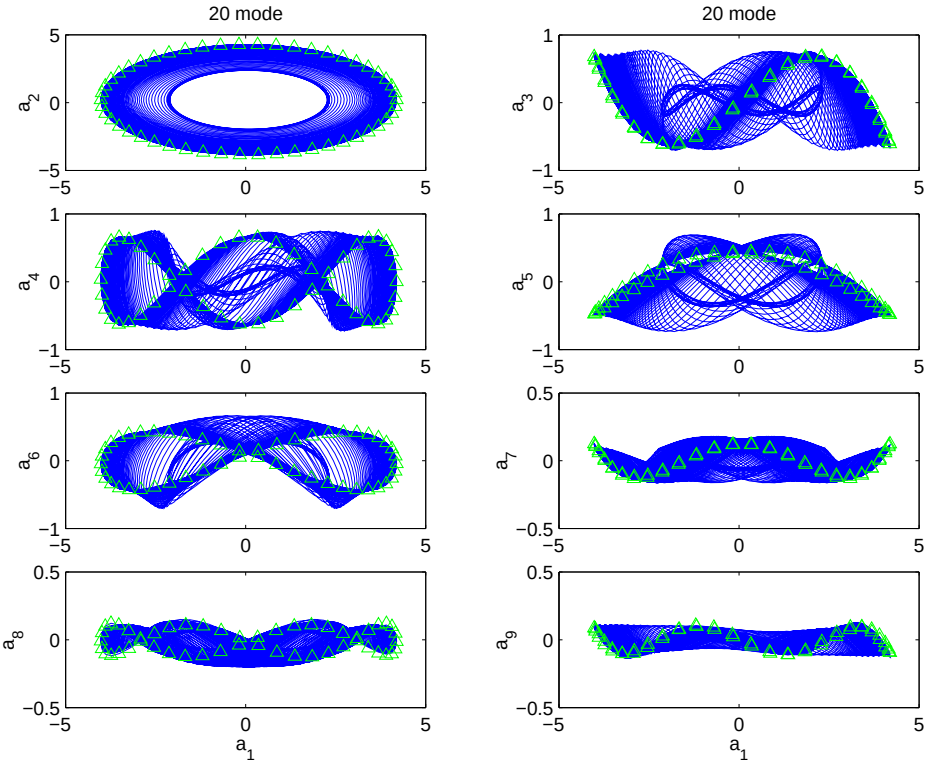

Fig. 16. $Re = 500$: Phase portrait of the first 9 modes in the 20-mode POD only system (lines) compared to the DNS data (symbols).

Acknowledgments

The first author gratefully acknowledges the DPST (Development and Promotion of Science and Technology Talents) project from Thailand for providing his scholarship during his graduate studies at Brown University. This work was supported by ONR, and computations were performed at the facilities of NCSA (U. Illinois) and at TCASV (Brown University). The authors would like to acknowledge helpful discussions with Dr. Ma Xia.

References

[1] G. Bekooz, P. Holmes, J. Lumley, The proper orthogonal decomposition in the analysis of turbulent flows, Ann. Rev. Fluid Mech. 25 (1993) 539–575.

[2] L. Sirovich, Turbulence and the dynamics of coherent structures, Parts I, II and III, Quart. Appl. Math. XLV (1987) 561–590.

[3] A. Glezer, Z. Kadioglu, A. Pearlstein, Development of an extended proper orthogonal decomposition and its application to a time periodically forced plane mixing layer, Phys. Fluids 1(8) (1989) 1363.

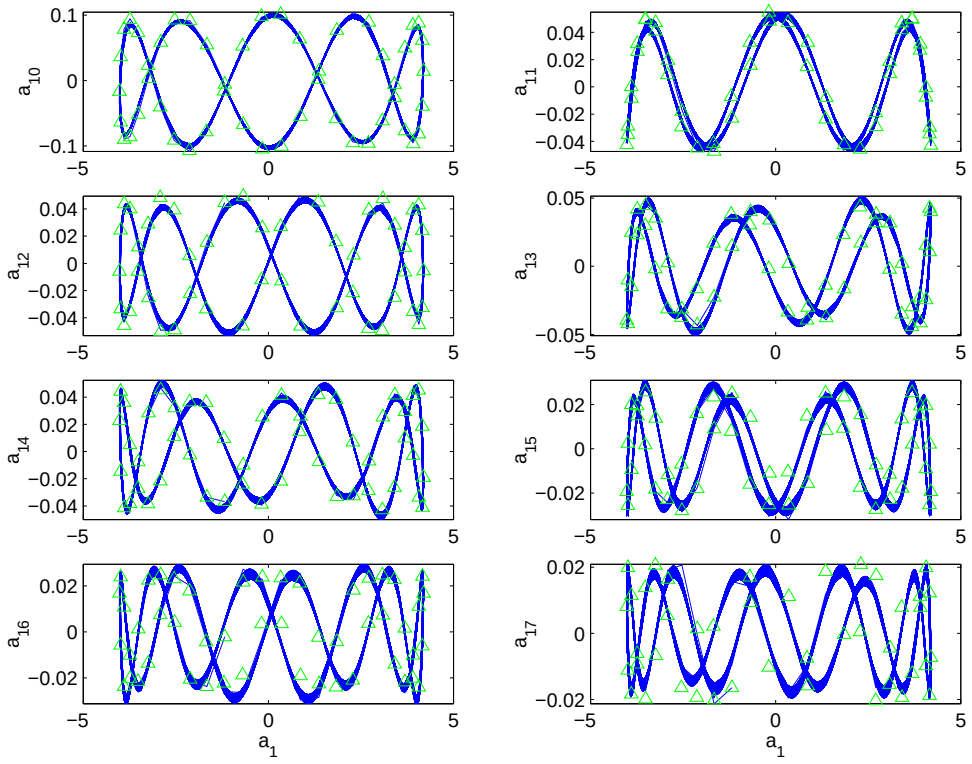

Fig. 17. $Re = 500$: Phase portrait of modes 10-17 in the 20-mode SVV-POD system (lines) compared to the DNS data (symbols).

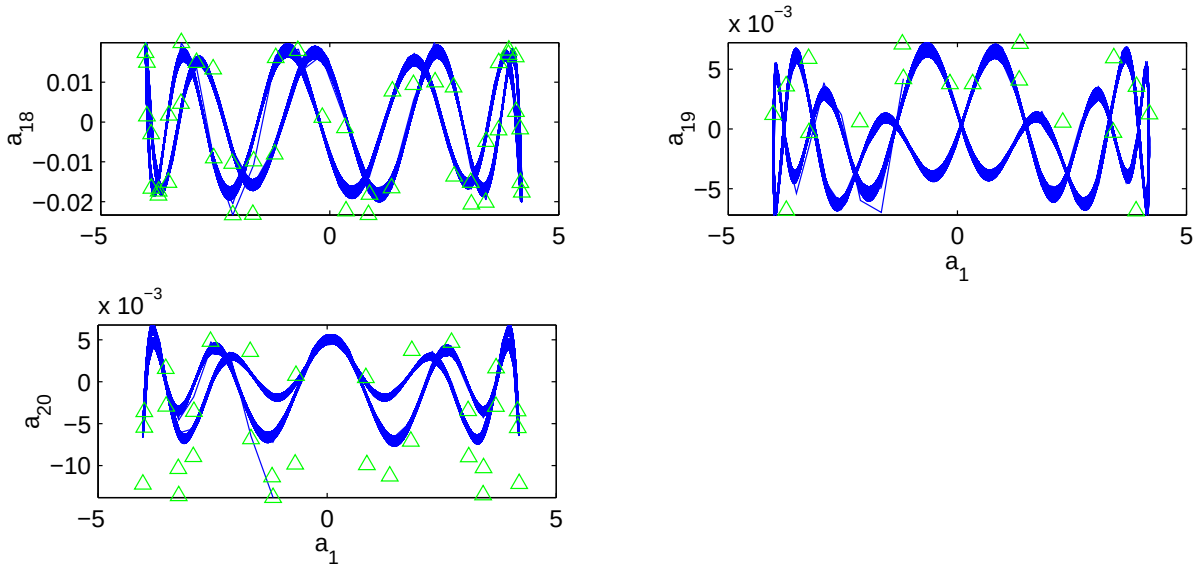

Fig. 18. $Re = 500$: Phase portrait of modes 18-20 in the 20-mode SVV-POD system (lines) compared to the DNS data (symbols).

[4] J. Citriniti, W. George, Reconstruction of the global velocity field in the axisymmetric mixing layer utilizing the proper orthogonal decomposition, J. Fluid Mech. 418 (2000) 137–166.

[5] R. Arndt, D. Long, M. Glauser, The proper orthogonal decomposition of pressure fluctuations surrounding a turbulent jet, J. Fluid Mech. 340 (1997) 1–33.

[6] S. Gordeyev, F. Thomas, Coherent structure in the turbulent planar jet. Part 1. Extraction of proper orthogonal decomposistion eigenmodes and their self-similarity, J. Fluid Mech. 414 (2000) 145–194.

[7] A. Deane, I. Kevrekidis, G. Karniadakis, S. Orszag, Low-dimensional models for complex geometry flows: Application to grooved channels and circular cylinders, Phys. Fluids A 3 (10) (1991) 2337–2354.

[8] N. Aubry, P. Holmes, J. Stone, J. Lumley, The dynamics of coherent structures in the wall region of a turbulent boundary layer, J. of Fluid Mech. 192 (1988) 115.

[9] D. Rempfer, H. Fasel, Evolution of three-dimensional coherent structures in a flat-plate boundary layer, J. of Fluid Mech. 260 (1994) 351.

[10] A. Liakopoulos, P. Blythe, H. Gunes, A reduced dynamical model of convective flows in tall laterally heated cavities, Proc. R. Soc. Lond. A 453 (1997) 663.

[11] W. Cazemier, R. Verstappen, A. Veldman, Proper orthogonal decomposition and low-dimensional models for driven cavity flows, Phys. Fluids 10 (7) (1998) 1685–1699.

[12] S. Singh, H. James, A. Gregory, B. Siva, K. James, Optimal feedback control of vortex shedding using proper orthogonal decomposition models, Trans ACME 123 (2001) 612–618.

[13] C. Foias, M. Jolly, I. Kevrekidis, E. Titi, Dissipativity of the numerical schemes, Nonlinearity 4 (1991) 591–613.

[14] M. Jolly, I. Kevrekidis, E. Titi, Preserving dissipation in approximate inertial manifolds for the kuramoto-sivashinsky equation: analysis and computations, J. Dynam. Diff. Eq. 3 (1991) 179–197.

[15] M. Marion, R. Temam, Nonlinear Galerkin methods, SIAM J. Numer. Anal 26 (1989) 1139–1157.

[16] A. Debussche, T. Dubois, R. Temam, The nonlinear Galerkin method: A multiscale method applied to the simulation of homogeneous turbulent flows, Theor. Comp. Fluid. Dyn. 7 (1995) 279–299.

[17] J. Shen, Long time stability and convergence for fully discrete nonlinear Galerkin methods, Applicable Anal. 38 (1989) 201–229.

[18] X. Ma, G. Karniadakis, H. Park, M. Gharib, DPIV-driven simulation: A new computational paradigm, Proc. R. Soc. Lond. A in press.

[19] E. Tadmor, Convergence of spectral methods for nonlinear conservation laws, SIAM J. Numer. Anal. 26(1) (1989) 30.

[20] G. Karamanos, G. Karniadakis, A spectral vanishing viscosity method for large-eddy simulations, J. of Comp. Phys. 162 (2000) 22–50.

[21] S. M. O. Kaber, A Legendre pseudospectral viscosity method, Journal of Computational Physics 128 (1996) 165.

[22] ∅. Andreassen, I. Lie, C. Wasberg, The spectral viscosity method applied to simulation of waves in a stratified atmosphere, Journal of Computational Physics 110 (1994) 257.

[23] E. Tadmor, Super viscosity and spectral approximations of nonlinear conservation laws, in: Numerical Methods for Fluid Dynamics, IV. M.J. Baines and K.W. Morton, eds., Clarendon Press, Oxford, 1993, p. 69.

[24] H.-P. Ma, Chebyschev-Legendre spectral viscosity method for nonlinear conservation laws, SIAM J. Numer. Anal. 35(3) (1998) 901.

[25] H.-P. Ma, Chebyschev-Legendre super spectral viscosity method for nonlinear conservation laws, SIAM J. Numer. Anal. 35(3) (1998) 903.

[26] X. Ma, G. Karniadakis, A low-dimensional model for simulating 3d cylinder flow, J. Fluid Mech. 458 (2002) 181–190.

[27] G. Karniadakis, S. Sherwin, Spectral/hp Element Methods for CFD, Oxford University Press, 1999.

[28] L. Sirovich, Turbulence and the dynamics of coherent structures, Part 1: Coherent structures, Q. Appl. Math. 45 (1987) 561.

[29] L. Sirovich, Turbulence and the dynamics of coherent structures, Part 2: Symmetries and transformations, Q. Appl. Math. 45 (1987) 573.

[30] L. Sirovich, Turbulence and the dynamics of coherent structures, Part 3: Dynamics and scalings, Q. Appl. Math. 45 (1987) 583.

[31] S. Sirisup, Convergence and stability of low-dimensional flow models, Ph.D. thesis, Division of Applied Mathematics, Brown University (in progress).

[32] M. Crandall, P. Lions, Viscosity solutions of Hamilton-Jacobi equations, Trans. Amer. Math. Soc. 61 (1983) 629.

[33] Y. Maday, S. O. Kaber, E. Tadmor, Legendre pseudospectral viscosity method for nonlinear conservation laws, SIAM J. Numer. Anal. 30 (1993) 321.

[34] E. Tadmor, Total variation and error estimates for spectral viscosity approximations, Math. Comp. 60 (1993) 245.

[35] R. Kraichnan, Eddy viscosity in two and three dimensions, J. Atmos. Sci. 33 (1976) 1521.

[36] M. Lesieur, O. Metais, New trends in large-eddy simulation, Ann. Rev. Fluid Mech. 28 (1996) 45.

[37] J. Chollet, Two-point closures as a subgrid scale modelling for large eddy simulations, in: Turbulent Shear Flows IV, ed. F. Durst and B. Launder, Lecure notes in Physics, Springer-Verlag, 1984.

[38] A. Bangia, P. Batcho, I. Kevrekidis, G. Karniadakis, Unsteady two-dimensional flows in complex geometries: Comparative bifurcation studies with global eigenfunction expansions, SIAM J. Sci. Comput. 18 (1997) 775–805.